ACS SyntheticBiology

pubs.acs.org/synthbio

Research Article

CRISPRi-Mediated NIMPLY Logic Gate for Fine-Tuning the Whole-Cell Sensing toward Simple Urine Glucose Detection

Shih-I Tan and I-Son Ng*

Cite This: *ACS Synth. Biol.* 2021, 10, 412–421

Read Online

ACCESS | Metrics & More | Article Recommendations | Supporting Information

ABSTRACT: Whole-cell biosensors have been regarded as a prominent alternative to chemical and physical biosensors due to their renewability, environmental friendliness, and biocompatibility. However, there is still a lack of noninvasive measurements of urine glucose, which plays a vital role in monitoring the risk of diabetes in the healthcare system, *via* whole-cell biosensors. In this study, we characterized a glucose-inducible promoter and further enhanced the sensing performance using three genetic effectors, which encompassed ribozyme regulator (RiboJ), clustered regularly interspaced short palindromic repeat interference (CRISPRi), and plasmid-based T7RNA polymerase (PDT7), to develop the noninvasive glucose biosensor by fluorescent signal. As a result, RiboJ increased dynamic range to 2989 au, but declined signal-to-noise (S/N) to 1.59, while CRISPRi-mediated NIMPLY gate intensified both dynamic range to 5720 au and S/N to 4.58. The use of single PDT7 orthogonal with T7 promoter in cells (*i.e.*, P strain) achieved a 44 180 au of dynamic range with S/N at 3.08. By coupling the PDT7 and NIMPLY-mediated CRISPRi, we constructed an optimum PIGAS strain with the highest S/N value of 4.95. Finally, we adopted the synthetic bacteria into a microdevice to afford an integrative and portable system for daily urine glucose inspection, which would be an alternative approach for medical diagnosis in the future.

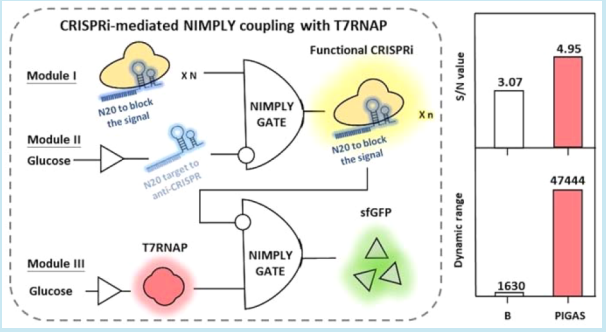

KEYWORDS: *glucose sensing, RiboJ, CRISPRi, T7RNAP amplifier, urine-based biosensor, noninvasive detection*

Genetically encoded whole-cell biosensors recently attracted increasing attention in the escalating era of synthetic biology since they are renewable, environmentally friendly, cost-effective, and biocompatible, such as *in situ* detection, when compared to the conventional physical and chemical biosensors.[1] Therefore, the whole-cell biosensor has been developed and applied in many different fields, including environmental protection,[2,3] medical and diagnostic applications,[4,5] and programmable bioprocess for chemical and protein productions.[6,7] Notably, for the medical application, *in situ* detection and simultaneous treatment of cancer cells could only be accomplished using the genetically encoded whole cell biosensors.[4,5] In this context, a high-performance whole-cell biosensor is vital and could be accomplished by directly tuning the strength, amounts, and types of genetic elements, such as the promoters, regulators, ribosome binding site (RBS), operons, plasmid copy numbers, and reporter genes.[8−10]

The central dogma of synthetic biology is to rewire cellular programs toward unprecedented functions, which highly relies on orthogonal genetic pairs. However, cellular reprogramming involved complex design, thus by incorporating the Boolean logic gates, which contained binary AND, OR, NOT, and NAND gates, it could be simplified and mimicked as electric circuits. Currently, Wan and his colleagues exhibited a three-cascade amplifier logic gate, which consisted of orthogonal pairs *hrp*RS/*hrp*L promoter as a unit, conferred improved detection limit and output up to 5000-fold and 750-fold, respectively.[1] By devising an AND with layer-AND logic gate to express individual orthogonal pairs, the high specificity and low false-positive rate of diagnosis could be achieved, respectively.[2] Besides, it has demonstrated a 15- and 9.2-fold enhancement on the sensing sensitivity of cadmium and lead by chromosomal integration of orthogonal pairs of T7 RNA polymerase (T7RNAP) and T7 promoter, respectively.[3] The plasmid-driven orthogonal T7 system also enhanced sensitivity of the copper ion with a 5.2-fold improvement.[11] With the exploration of novel transcriptional factors and orthogonal pairs, a complex logic gate could be designed for a precise detection.[12,13] However, it required the balance of multiple orthogonal pairs, thus reducing the cell burden. Fortunately, with the assistance of the recently surging clustered regularly interspaced short palindromic repeat interference (CRISPRi) technology, it has been demonstrated a simple design of AND

Received: January 12, 2021
Published: February 9, 2021

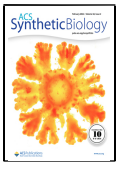

https://dx.doi.org/10.1021/acssynbio.1c00014
ACS Synth. Biol. 2021, 10, 412–421

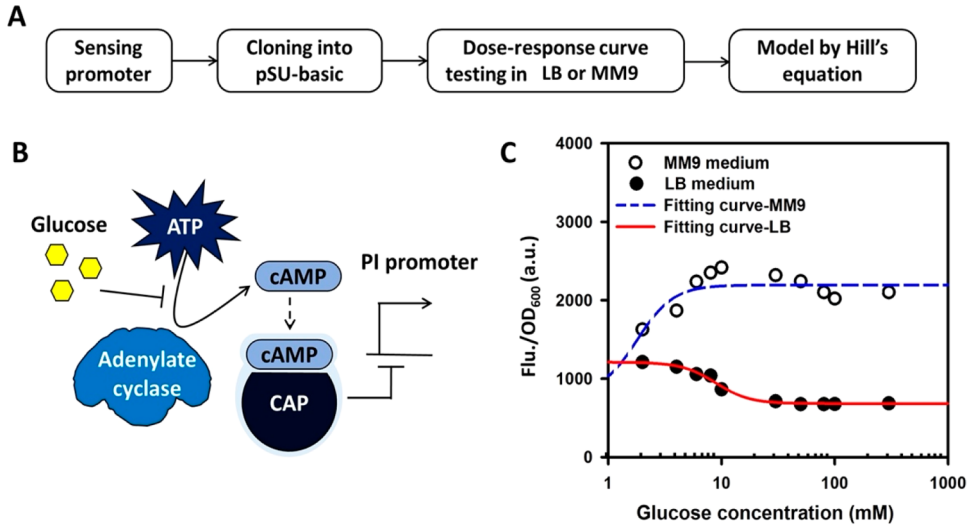

Figure 1. Performance of PI glucose sensing promoter in LB or MM9 medium. (A) flowchart of parameter determination, (B) sensing mechanism, and (C) dose−response curve. The white and black circles are the data of specific fluorescence intensity under the induction of different glucose concentrations in MM9 and LB medium, respectively. The blue dashed line and red solid line is the fitting curve based on the Hill's equation.

and NAND gate by modular expression of dead effectors (*i.e.*, dCad9) and sgRNA.[14] Therefore, it is more possible to design a complex logic gate design for high-performance whole-cell biosensing.

Due to the profound changes in diet and lifestyle, diseases of civilization such as coronary heart disease, obesity, hypertension, and diabetes have extensively affected human beings. Among these diseases, diabetes has been one of the top ten mortal diseases in the past two decades.[15] Thus, efforts put on the invasive blood-based[16] or noninvasive urine-based glucose monitors have been worthy of development.[17] The technology for invasive blood-based glucose detection is considerably more mature but dangerous for the patients in long-term applications. In contrast, the noninvasive measurement is more preferable to the patients due to the wound-free, painless, and convenient process and principally depends on enzyme-coated electrodes.[18] However, there are still no precise and user-friendly approaches by using whole-cell chassis as biosensor to monitor the real-time signal. Besides, the urine-based glucose detection *via* synthetic biology is still limited.

Deciphering the combinatorial effect of multiple genetic effectors can afford a new insight into high-performance whole-cell biosensors for noninvasive detection of urine glucose as a management and prevention of diabetes. The noninvasive detection provided a convenient and woundless process for daily measurement, which is an important record and early symptom for tracking the risk of diabetes. In this study, we aimed to adopt three individual genetic effectors, including the ribozyme regulator (RiboJ), CRISPRi, and T7RNAP, as well as the combinatorial effect based on the glucose-inducible promoter, thus to create a more precise and portable glucose biosensor. Eventually, we developed a portable microdevice that used the synthetic glucose-sensing bacteria in a microscopic sensing level as a more practical application.

RESULTS AND DISCUSSION

Determining Medium for Whole-Cell Glucose Sensing. In order to characterize the sensing promoter, we designed a flowchart (Figure 1A) where the promoter was constructed into a high copy number plasmid (*i.e.*, pSU plasmid), and the inspection of dose−response curve was performed using LB and MM9 medium. The data were fitted by Hill's equation to determine the sensing performance. Actually, the high-copy plasmids have been proven to afford a superior performance of whole-cell biosensors.[19] Herein, we characterized the PI promoter, which was an activatable promoter controlled by glucose. As shown in Figure 1B, PI promoter was in the "OFF" state when the glucose was absent because the catabolite activation protein (CAP) bound with the intrinsic cAMP blocked the PI promoter and inhibited the transcription of the downstream gene. In contrast, if glucose existed, the reduction of cAMP caused by the glucose-induced inhibition of adenylate cyclase would alleviate the binding of CAP to PI promoter, thus turning "ON" the PI promoter. The dose−response curve showed that the sensing performance of B strain (*i.e.*, glucose-sensing basic) in MM9 was better than that in LB medium, suggesting the complex nutrients in LB medium raised an intricate metabolism. Hence, the B strain displayed an abnormal dose curve (Figure 1C) and a negative Hill's coefficient in LB medium (*i.e.*, *b* value of −2.9 in Table 1). Besides, it has been reported that the amounts and activity of cAMP and CAP would be influenced by different chemicals and regulated *via* various gene expressions, which further supported our result of an inverse dose−response curve in the LB medium.[20,21] For glucose sensing in the MM9 medium, it showed a 1403 au dynamic range of *a* and the specific fluorescence saturated around 10 mM glucose, resulting in a relatively low EC_{50} value (*i.e.*, parameter *c*) of 1.81 mM glucose (Table 1). According to PI promoter is saturated at 10 mM of glucose and the study by Ito and his colleagues, a urine glucose

Table 1. Modeling Parameters of Hill's Equation for Glucose Sensing in LB and MM9 Medium[a]

medium	y_0 (au)	*a* (au)	*b*	*c* (mM)	R^2
LB	681	528	−2.9	8.88	0.9885
MM9	792	1403	2.7	1.81	0.8951

[a] y_0 represents the basal or leakage expression of the inducible promoter; *a* is the dynamic range; *b* is the Hill coefficient; *c* represents the concentration resulting in half-maximal induction.

https://dx.doi.org/10.1021/acssynbio.1c00014
ACS Synth. Biol. 2021, 10, 412−421

concentration of 10 mM indicated a high risk of diabetes.[22] Thus, we performed the glucose concentration at 0 and 10 mM for individual and combinatory genetic effectors in the following.

Actually, the sensing medium significantly affected the whole-cell sensing performance. For example, Chen and his colleagues demonstrated that the defined MM9 medium resulted in a lower detection limit of putrescine due to rapid uptake of putrescine as the major nitrogen source.[23] In our glucose sensing system, the better sensing performance in MM9 was ascribed to the quicker uptake rate of glucose than that in LB because glucose was the major carbon source in MM9 medium.

Enhancing the Glucose Sensing Efficacy by Ribozyme Regulator RiboJ. A wide dynamic range affords a more receptive biosensor; thus, we added a ribozyme regulator RiboJ between the ribosome binding site (*i.e.*, B0034 from iGEM) and PI promoter (Figure 2A and 2B), because the RiboJ has

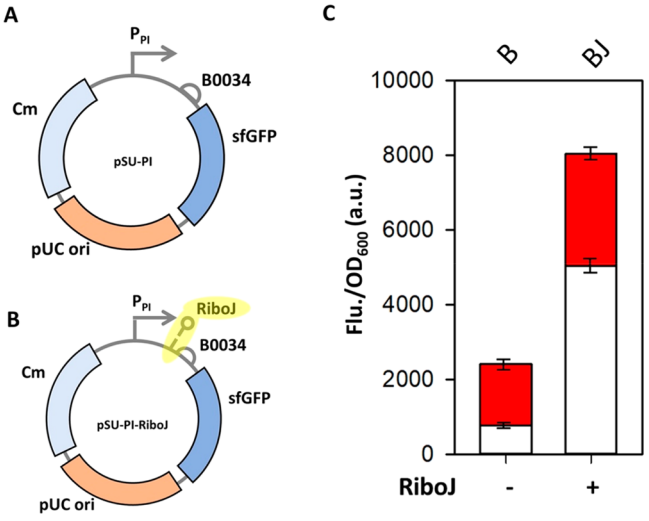

Figure 2. RiboJ effect in the glucose sensing. Map of (A) pSU-PI-sfGFP and (B) pSU-PI-RiboJ-sfGFP. (C) The specific fluorescence intensity of DH5α harboring pSU-PI-sfGFP (*i.e.*, B strain) and pSU-PI-RiboJ-sfGFP (*i.e.*, BJ) with (red bar) or without (white bar) induction of 10 mM glucose. Error bars represented the s.d. (standard deviation) of three independent experiments (n = 3).

been reported to enhance both transcriptional and translational level of the downstream gene.[24] As shown in Figure 2C, after the addition of the RiboJ in the plasmid, all the specific fluorescence intensity increased, no matter whether the glucose was induced at 10 mM (red bars) or not (white bars), and it showed a more acute leakage expression level of 5052 au in BJ strain when compared to that of 787 au in B strain (Table 2). As 10 mM glucose was presented, the specific fluorescence intensity of BJ strain increased to 8048 au Therefore, the dynamic range elevated from 1630 au to 2989 au. However, if considering the signal-to-noise ratio (S/N), the addition of RiboJ would pose an adverse effect, in which S/N value declined from 3.07 to 1.59 (Table 2).

In the timeline of RiboJ development, it was first applied to prevent the interference of the genetic context from evaluating the strength of different promoters. Because the RNA sequence in front of the RiboJ sequence would be cleaved, the standardized 5′ leader was remained to make precise identification of the promoter strength.[25] Clifton and his

Table 2. Summary of Sensing Efficacy Using Different Genetic Effectors

		fluorescence/OD_{600} (au)			
		glucose			
strain	genetic effectors	0 mM	10 mM	dynamic range[a]	signal-to-noise ratio (S/N)[b]
B	–	787	2417	1630	3.07
BJ	RiboJ	5052	8041	2989	1.59
BICAC	CRISPRi	1538	7258	5720	4.58
P	PDT7	21254	65434	44180	3.08
PICAC	PDT7 and CRISPRi::CAP	9564	31982	22418	3.34
PIG	PDT7 and CRISPRi::sfGFP	5376	18622	13246	3.46
PIGAC	PDT7 and CRISPRi::sfGFP/anti-dCas9sg	5341	25488	20147	4.77
PIGAS	PDT7 and CRISPRi::sfGFP/anti-SynPsg	12016	59460	47444	4.95

[a]The dynamic range was calculated by subtraction of the fluorescence/OD_{600} at 10 mM and 0 mM glucose. [b]The signal-to-noise ratio (S/N) was calculated by division of the fluorescence/OD_{600} at 10 mM and 0 mM glucose.

colleague unexpectedly found not only that RiboJ insulated the genetic context, but also the hairpin structure of RiboJ could enhance both the mRNA stability and RBS activity.[24,26] Thus, the fluorescence intensity driven by the various constitutive promoter increased after the addition of RiboJ. Herein, we demonstrated the effect of RiboJ in an inducible system and showed that the addition of RiboJ in a glucose inducible system consistently increased the fluorescence intensity; however, the S/N value decreased.

Using CRISPRi System to Elevate S/N Value of Glucose Sensing. With the highly accessible design of CRISPRi,[27,28] we conceived that the CRISPRi could be used to reduce basal expression, thus enhancing the S/N value. The first CRISPRi was designed to target an essential gene, *can* gene, to offer a survival stress that would make cells express less sfGFP due to the cell growth being controlled by CRISPRi on *can* gene.[29] As considering the dynamic range, the specific fluorescence must be recovered by releasing the inhibition from CRISPRi, a glucose-induced anti-CRISPRi system was designed. In such context, our genetic design was divided into three modules (Figure 3A) and could be analogue to electric circuit (Figure 3B). First, module I was established for the functional CRISPRi targeting on essential gene to provide survival stress, whose design encompassed a constitutively expressed dCas9 as well as a sgRNA targeting to the promoter region of *can* essential gene. The sgRNA was driven by a synthetic promoter which has been used in CRISPRi.[29] Second, module II was the glucose-inducible antisense sgRNA to release the survival stress from module I when glucose existed in the environment. As shown in Figure S1, NIMPLY gate was used to illustrate the relationship between binary input and output, in which the output signal (*i.e.*, functional CRISPRi) occurred only when the A input (*i.e.*, module I) was presented with the absence of B input (*i.e.*, module II). Thus, combined module I and module II would form a NIMPLY gate to generate a functional CRISPRi system (Figure 3B). Third, module III was the glucose-inducible

https://dx.doi.org/10.1021/acssynbio.1c00014
ACS Synth. Biol. 2021, 10, 412−421

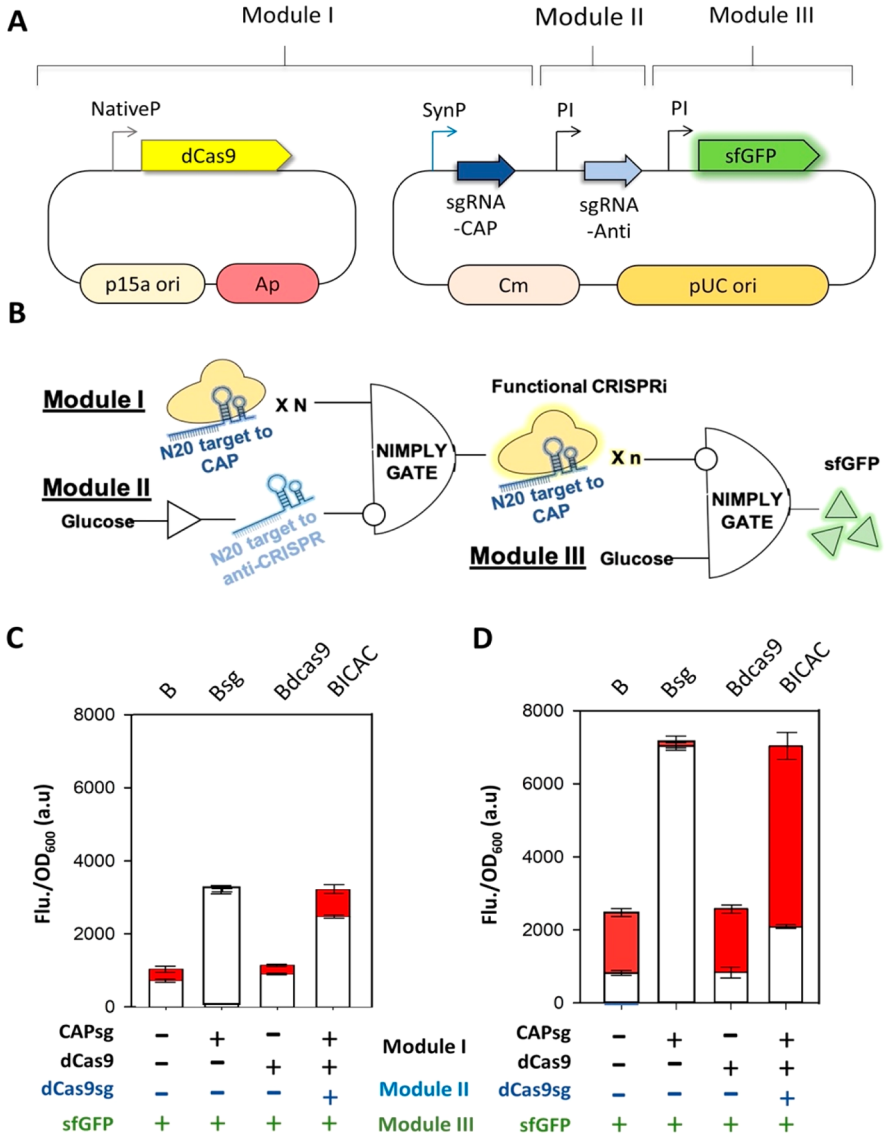

Figure 3. CRISPRi effect in the glucose sensing system. (A) Design of CRISPRi system. Two plasmids were used and divided into three modules. Module I, II, and III were CRISPRi-CA for conferring survival stress, anti-CRISPRi-CA for releasing the survival stress and fluorescence expression cassettes, respectively. (B) Simplified diagram analog to the electronic circuits to illustrate the CRISPRi effect. The specific fluorescence intensity of B strain and other strains harboring different CRISPRi system (*i.e.*, Bsg, Bdcas9, and BICAC) with (red bar) or without (white bar) induction of 10 mM glucose at (C) 2 h and (D) 12 h. Error bars represented the s.d. (standard deviation) of three independent experiments (n = 3).

sfGFP cassette to offer the signal. For the complete design of CRISPRi, two NIMPLY gates were harnessed to reduce the leakage expression and to remain the high fluorescence at 10 mM glucose. Afterward, we examined the biosensing by measuring the fluorescence intensity and biomass at 2 h (Figure 3C) and 12 h (Figure 3D). First, we assessed the effect of module II in the glucose sensing system (*i.e.*, Bsg and BdCas9 strains). At 2 h, sgRNA targeted on CAP (*i.e.*, Bsg) unexpectedly increased the fluorescence intensity and reduced the dynamic range between the condition with or without 10 mM glucose induction. We supposed that our plasmid design on the strong synthetic promoter located at 119 bp in front of the sfGFP coding region resulted in the overtranscription of sfGFP, thus increasing the expression of sfGFP and decreasing the dynamic change. On the contrary, coexpression of dCas9 (*i.e.*, BdCas9) would not affect glucose biosensing. By coupling module I, II, and III to form the completed CRISPRi-mediated NIMPLY gate, it showed a reduced basal expression (*i.e.*, without glucose induction), and the specific fluorescence at 10 mM glucose remained at the same level as comparing BICAC to Bsg strain, which further proofed our original design and concept. For the fluorescence intensity at 12 h, it showed a similar trend in each strain, but the fluorescence dynamic range increased. The CRISPRi system with antisense on dCas9 (*i.e.*, BICAC strain) successfully enhanced both the dynamic range and S/N value to 5720 au and 4.58, respectively (Table 2).

Actually, CRISPR technology originated from the bacteria immune system and has been already developed as an efficient genome editing tool. With the assistance of the structural study, the active domain of the Cas9 protein was replaced to form a deactivated Cas9 that could strongly bind to the targeted sequence without breaking the double strain DNA, termed CRISPR interference (CRISPRi).[30−32] CRISPRi system has been widely applied in the researches regarding synthetic biology, including phenotype mapping, gene locus localization, carbon flux redirection, and biosensor.[13,33] Among

https://dx.doi.org/10.1021/acssynbio.1c00014
ACS Synth. Biol. 2021, 10, 412−421

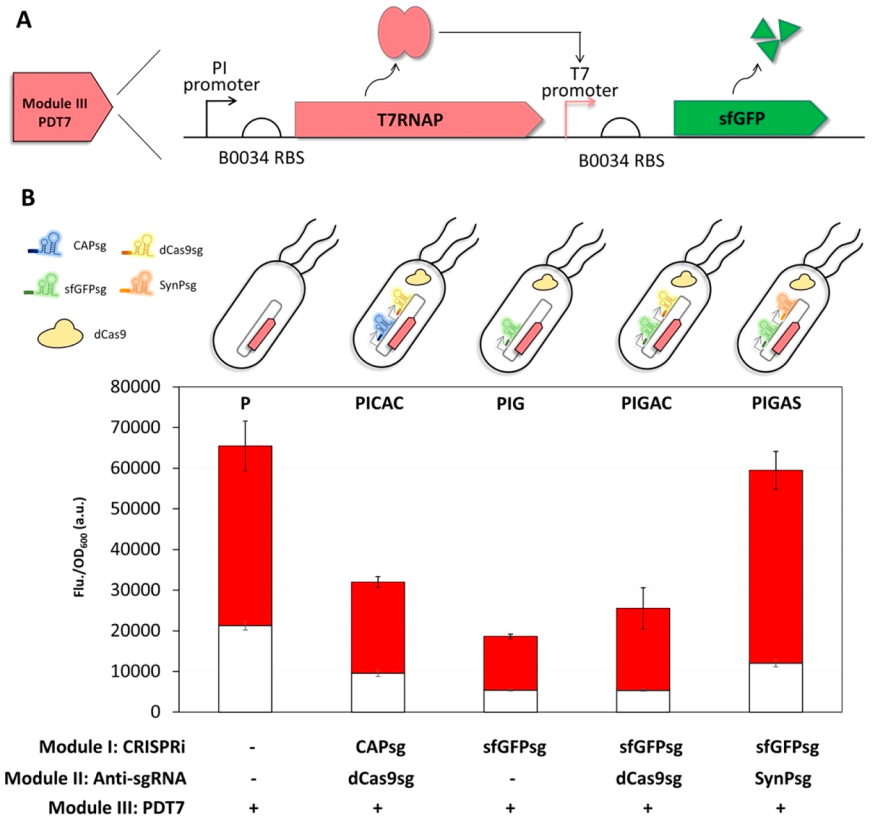

Figure 4. Coupling the plasmid-driven T7 system (PDT7) with CRISPRi to boost the sensing performance of whole-cell glucose sensing. (A) The genetic design of module III which T7RNAP was driven by the PI glucose-inducible promoter and the fluorescence signal was driven by the T7 promoter. (B) The specific fluorescence intensity of different strains including P, PICAC, PIG, PIGAC, and PIGAS with (red bar) or without (white bar) 10 mM glucose induction. The error bars represented the s.d. (standard deviation) of three independent experiments (n = 3).

the application of CRISPRi in biosensors, most of the successful cases depended on directly targeting the reporter gene by an inducible dCas9 or sgRNA, thus establishing a "TURN OFF" type biosensor. In this study, we conceived a new concept that the reduced fluorescence could be achieved by a survival threat from inhibition of essential gene, which was inspired by the powerful adaptive laboratory evolution (ALE) that the cell would spare no energy to survive when being threatened.[34] Furthermore, the three modules system, including the CRISPRi, antisense RNA and fluorescence, to form the CRISPRi-mediated NIMPLY gate could be used to establish a "TURN ON" type whole-cell biosensor. Actually, it has been also demonstrated as a switchable and programmable bioprocessing,[35] while the design of antisense RNA in the literature was more complex than that in our study. On the other hand, our study demonstrated the first attempt to enhance the whole-cell sensing performance by CRISPRi-mediated NIMPLY gate.

Applying PDT7 and CRISPRi to Boost Glucose Sensing Performance. As an ambitious desire to explore a highly sensitive glucose whole-cell biosensor, T7RNAP and T7 promoter orthogonal pairs were used as it has been reported to confer a strong expression of the downstream genes.[36,37] The two orthogonal pairs were inserted between the PI promoter and sfGFP to obtain P strain (Figure 4A), and the results showed that the specific fluorescence intensity increased surprisingly, and the dynamic range raised from 1630 au for B strain to 44 182 au for P strain, a 27-fold enhancement (Figure 4B, P strain) without the adverse effect on S/N value (Table 2).

Next, the CRISPRi system was incorporated with the T7 system to be PICAC strain to explore higher-performance whole-cell glucose biosensor. However, this strain showed a decrease in the specific fluorescence intensity of basal expression and also at 10 mM-glucose induction (Figure 4B, PICAC). Precisely, the dynamic range reduced to 22 418 au, but the S/N value increased slightly from 3.08 to 3.34 (Table 2). It indicated the designed CRISPRi could efficiently reduce the leakage in expression, but the antisense worked ineffectively in the T7 system due to the serious stress from the CRISPRi and PDT7. Our previous publication also clarified that the PDT7 system would require intensive energy for gene expression.[11] Therefore, we redesigned the sgRNA to the sfGFP to directly repress the sfGFP expression instead of the cell growth (*i.e.*, CAPsg). When coupling the sfGFPsg and PDT7 in PIG strain, both the florescence intensity obtained from the condition with or without glucose decreased, which demonstrated the function of CRISPRi on the reduction of sfGFP expression (Figure 4B, PIG strain). Incorporation of antisense sgRNA on dCas9 in PIG to form PIGAC increased the fluorescence intensity from 18 622 au to 26 488 au at 10 mM glucose with a lower leakage. PIGAC achieved higher S/N value, while the dynamic range was still lower than that in P strain (Figure 4B, PIGAC strain). Thus, we considered to repress the sgRNA expression, instead of dCas9 protein expression, to release the function of the CRISPRi (Figure 4B, PIGAS strain). Surprisingly, alteration of antisense sgRNA from anti-dCas9 to anti-SynP led to a higher S/N of 4.95 and recovery of dynamic range to 47 444 a.u (Table 2). We

https://dx.doi.org/10.1021/acssynbio.1c00014
ACS Synth. Biol. 2021, 10, 412−421

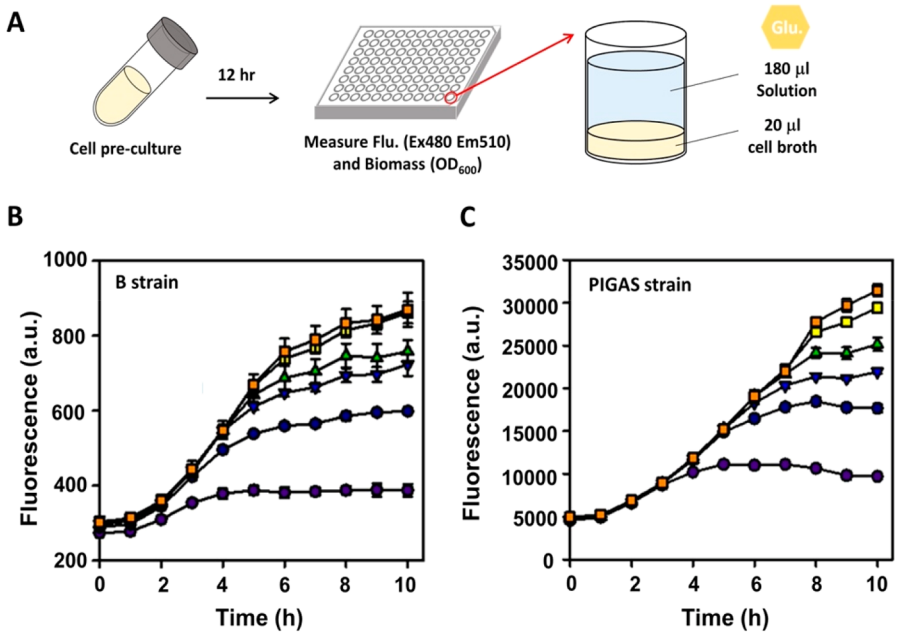

Figure 5. Microsystem for real-time glucose biosensing. (A) Procedure of the microsystem biosensing and the component in the well. Fluorescence intensity of (B) B strain and (C) PIGAS strain. The curve with purple, cyan, blue, green, yellow, and orange color indicated the different concentration of 0, 2, 4, 6, 8, 10 mM glucose. The error bars represented the s.d. (standard deviation) of three independent experiments (n = 3).

provided a paradigm to optimize the whole-cell biosensor by using T7RNAP and NIMPLY-mediated CRISPRi.

Adapting Synthetic Bacteria into a Portable Urine Glucose Sensing System. The B and PIGAS strains were applied in a 96-microwell plate to demonstrate the feasibility of real time detection using whole-cell biosensing (Figure 5A). The cell was first cultured in the tube for preculture and then inoculated 20 μL into a well containing 180 μL sensing medium for further examination. As shown in Figure 5B, the fluorescence would increase along with time in B strain, and the final fluorescence intensity at 10 h only elevated to 380 au at 0 mM and 870 au at 10 mM glucose. The PIGAS strain manifested a comparable behavior as B strain, but the fluorescence intensity increased from 870 au for B (Figure 5B) to 32 145 au for PIGAS at 10 h (Figure 5C). The signal of fluorescence has increased 30-folds when used PIGAS for glucose sensing. These results also showed that the real-time monitoring is available in the microsystem.

As considering the selectivity, we immersed the B and PIGAS strain into different kinds of the sugars (*i.e.*, xylose, arabinose, and lactose) and tested the fluorescence. As shown in Figure 6A, all fluorescence intensities of B strain were relatively low (Figure 6A, yellow bars) but have significantly enhanced in PIGAS strain (Figure 6A, orange bars). For the xylose and arabinose, the S/N value was only around 1.5, which is relatively low when compared to the S/N value of 3.2 and 4.9 in glucose from B and PIGAS strains, respectively. While the 10 mM lactose was presented, the S/N could reach 2.8 and 3.0 for B and PIGAS strains because the lactose was disaccharide composed of glucose and galactose. The results showed that PI promoter strongly and stringently responded to the glucose molecules and the selectivity of different sugars, which was ranked from glucose > lactose > xylose = arabinose. This indicated the precision of glucose detection *via* PI promoter, especially in PIGAS (Figure 6A).

Next, we incubated our synthetic bacteria B and PIGAS strain in the artificial urine with or without 10 mM glucose to inspect the florescence intensity. Two kinds of devices were used at first, where a tube-based device was a 15 mL plastic tube containing 3.2 mL artificial urine, while a well-based device contained 180 μL artificial urine. There was no significant difference when B strain was used in both devices (Figure 6B). Actually, MM9 medium and artificial urine were at pH 7 and pH 5, respectively. According to the previous study, the sfGFP intensity was influenced by pH environment and reduced 55% at pH 5.[38] Thus, the poorer fluorescent signal in the artificial urine was attributed to the low pH value. Ultimately, we reckoned that the fluorescence intensity demands an expensive detector to measure it, and thus a membrane-based device equipped with a blue LED flashlight was devised (Figure 6C). It was divided into three sections: (a) the upper section was used to incubate the synthetic bacteria in urine for biosensing; (b) the lower section was employed to store the wasted urine; (c) bacteria on the membrane were detected by blue LED flashlight and sfGFP was observed (Figure 6C, left). The B strain did not present eye-detectable fluorescence even with the 10 mM glucose, while fluorescence and a significant difference were easily observed by the eye when the PIGAS strain was used (Figure 6C, right).

Otten and her colleagues recently utilized the FRET-based method to quantify the glucose concentration in the medium and demonstrated a precise measurement, but it required the purification of the FRET-sensor protein and a sample size was in milliliter level.[39] We have successfully applied a CRISPRi-mediated NIMPLY gate to increase the dynamic range and S/N value for glucose detection in urine. Our membrane-based device provided a low-cost, simple, convenient, and portable platform for daily examination. Besides, we developed a modest, macroscopic way to determine the risk of diabetes, since a clear fluorescence signal was observed by the eyes, which was friendlier for diabetes patients. This biosensor technique not only empowers the management of urine glucose for diabetic patients, but also can be applied for

https://dx.doi.org/10.1021/acssynbio.1c00014
ACS Synth. Biol. 2021, 10, 412−421

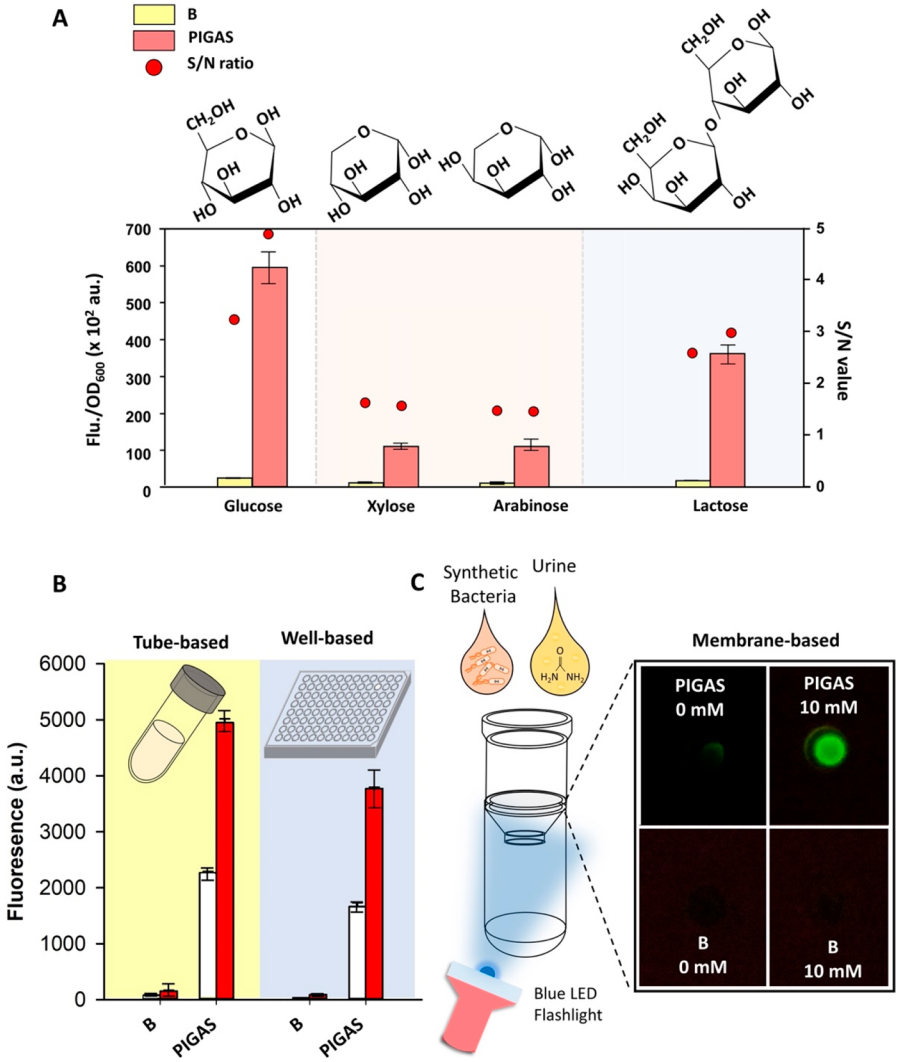

Figure 6. Application and comparison between B and PIGAS as the synthetic whole-cell biosensor. (A) Selectivity test in terms of specific fluorescent intensity (*Y*-axis in left, bars) and S/N value (*Y*-axis in right, dots) in different saccharides of glucose, xylose, arabinose, and lactose at 10 mM between B and PIGAS. (B) Fluorescence intensity in tube-based and well-based system, with (red bar) or without (white bar) 10 mM glucose. (C) Application and vision of the synthetic B and PIGAS strains in a microdevice for glucose detection of artificial urine used the blue LED flashlight. The error bars represented the s.d. (standard deviation) of three independent experiments (n = 3).

detection of more chemicals through the synthetic and logical design of genetic elements in the future.

MATERIALS AND METHODS

Strains, Plasmids, Primers, and Medium. The *E. coli* strains and plasmids used in this study are listed in Table 3 and Table 4, respectively. The sequences of used primers are listed in Table S1. *E. coli* DH5α was used as a cloning and glucose sensing host. Luria−Bertani (LB) medium (10 g/L tryptone, 10 g/L NaCl and 5 g/L yeast extract) was used for regular cultivation and MM9 medium (12.8 g/L Na_2HPO_4, 3 g/L KH_2PO_4, 0.5 g/L NaCl, 1 g/L NH_4Cl, 0.24 g/L $MgSO_4$, 0.011 g/L $CaCl_2$ and 4 g/L glucose) supplemented with corresponding antibiotics was used as basal medium for glucose sensing. The sequence of the genetic element used in this study is listed in Table S2.

Plasmid Construction. All the constructions were based on the conventional restriction-ligation method. For the construction of pSU-PI-sfGFP, the PI promoter was obtained by primer pairing and phosphorylation to expose the stick end

Table 3. Strains Used in This Study

strains	descriptions
E. coli DH5α	F-, Δ(*arg*F-*lac*)169, φ80d*lacZ*58(M15), Δ*pho*A8, *gln*X44(AS), λ-, *deo*R481, *rfb*C1, *gyr*A96(*Nal*R), *rec*A1, *end*A1, *thi*E1, *hsd*R17
B	DH5α harboring pSU-PI-sfGFP
BJ	DH5α harboring pSU-PI-RiboJ-sfGFP
Bsg	DH5α harboring pSUI-SynP-CAPsg-PI-sfGFP
Bdcas9	DH5α harboring pSU-PI-sfGFP and pSM-dCas9::Ap
BICAC	DH5α harboring pSUI-SynP-CAPsg-PI-anti-dCas9sg-sfGFP and pSM-dCas9::Ap
P	DH5α harboring pSU-PI-PDT7
PICAC	DH5α harboring pSUI-SynP-CAPsg-PI-anti-dCas9sg-PDT7 and pSM-dCas9::Ap
PIG	DH5α harboring pSUI-SynP-sfGFPsg-PI-PDT7 and pSM-dCas9::Ap
PIGAC	DH5α harboring pSUI-SynP-sfGFPsg-PI-anti-dCas9sg-PDT7 and pSM-dCas9::Ap
PIGAS	DH5α harboring pSUI-SynP-sfGFPsg-PI-anti-SynPsg-PDT7 and pSM-dCas9::Ap

https://dx.doi.org/10.1021/acssynbio.1c00014
ACS Synth. Biol. 2021, 10, 412−421

Table 4. Plasmids Used in This Study

plasmids	descriptions	remark
pSU-T7-sfGFP	2922 bp, Cm^R, pUC ori, T7 promoter, B0034 RBS, sfGFP	11
pSU-PI-sfGFP	2935 bp, Cm^R, pUC ori, PI promoter, B0034 RBS, sfGFP	This study
pSU-PI-RiboJ-sfGFP	3016 bp, Cm^R, pUC ori, PI promoter, RiboJ, B0034 RBS, sfGFP	This study
pSM-dCas9::Ap	9406 bp, Ap^R, p15a ori, dCas9, mobilization cluster	29 Addgene #154307
pSUI-SynP-CAPsg	3578 bp, Cm^R, pUC ori, Synthetic promoter (SynP), CAP-sgRNA (CAPsg), LacI	29 Addgene #154344
pSUI-SynP-CAPsg-PI-sfGFP	4365 bp, Cm^R, pUC ori, SynP promoter, CAPsg, PI promoter, B0034 RBS, sfGFP, LacI	This study
pSU-PI-anti-dCas9sg-sfGFP	3086 bp, Cm^R, pUC ori, PI promoter, anti-dCas9 sgRNA (anti-dCas9sg), B0034 RBS, sfGFP	This study
pSU-PI-anti-SynPsg-sfGFP	3086 bp, Cm^R, pUC ori, PI promoter, anti-synthetic promoter sgRNA (anti-SynPsg), B0034 RBS, sfGFP	This study
pSUI-SynP-CAPsg-PI-anti-dCas9sg-sfGFP	4516 bp, Cm^R, pUC ori, SynP-CAPsg, PI promoter, anti-dCas9sg, B0034 RBS, sfGFP, LacI	This study
pSU-PI-PDT7	5782 bp, Cm^R, pUC ori, PI promoter, B0034 RBS, T7RNAP, T7 promoter, sfGFP, Terminator	This study
pSUI-SynP-CAPsg-PI-anti-dCas9sg-PDT7	7363 bp, Cm^R, pUC ori, SynP-CAPsg, PI promoter, anti-dCas9sg, B0034 RBS, T7RNAP, T7 promoter, sfGFP, Terminator, LacI	This study
pSUI-SynP-sfGFPsg	3578 bp, Cm^R, pUC ori, SynP promoter, sfGFP-sgRNA (sfGFPsg), LacI	This study
pSUI-SynP-sfGFPsg-PI-PDT7	7079 bp, Cm^R, pUC ori, SynP promoter, sfGFPsg, PI promoter, B0034 RBS, T7RNAP, T7 promoter, sfGFP, Terminator, LacI	This study
pSUI-SynP-sfGFPsg-PI-anti-dCas9sg-PDT7	7230 bp, Cm^R, pUC ori, SynP promoter, sfGFPsg, PI promoter, anti-dCas9sg, B0034 RBS, T7RNAP, T7 promoter, sfGFP, Terminator, LacI	This study
pSUI-SynP-sfGFPsg-PI-anti-SynPsg-PDT7	7230 bp, Cm^R, pUC ori, SynP promoter, sfGFPsg, PI promoter, anti-SynPsg, B0034 RBS, T7RNAP, T7 promoter, sfGFP, Terminator, LacI	This study

of *Xba*I and *Bam*HI, and the vector was obtained from the digestion of pSU-T7-sfGFP by *Xba*I and *Bam*HI. For the pSU-PI-RiboJ-sfGFP, the RiboJ fragment was obtained from self-amplification by three primers (*Bam*HI-RiboJ-F1, RiboJ-R2, and *Hind*III-B0034-RiboJ-R3) and digestion of *Bam*HI and *Hind*III. Afterward, the RiboJ fragment was ligated into the *Bam*HI/*Hind*III-digested pSU-PI-sfGFP. For pSU-PI-PDT7, the vectors (*i.e.*, pSU-PI-sfGFP) were digested by *Hind*III and *Pst*I, and two inserts including the T7RNAP and T7-sfGFP cassette were obtained from amplifying from the Biobrick BBa_1450004 using *Hind*III-T7RNAP-F and *Spe*I-Terminator-T7RNAP-R and digestion of pSU-T7-sfGFP by *Xba*I and *Pst*I, respectively. For the CRISPRi system, all the sgRNAs were amplified from pSUI-SynP-CAPsg using *Bam*HI-N20-F and *Pst*I-*Spe*I-scaffold-R. Plasmids with the anti-CRISPR-sgRNA were cloned in two steps. First, the anti-CRISPR-sgRNA (*i.e.*, dCas9sg and SynPsg) and fluorescence expression cassettes (*i.e.*, PI-sfGFP and PI-PDT7 from pSU-PI-sfGFP and pSU-PI-PDT7) were cloned into the pSU-PI, where the pSU-PI-sfGFP was digested by *Bam*HI and *Pst*I as vector and the two inserts of the anti-CRISPR-sgRNA and fluorescence expression cassettes were digested by *Bam*HI/*Spe*I and *Xba*I/*Pst*I, respectively. Second, because the first construction has led to the ligation of anti-CRISPR sgRNA and fluorescence expression cassettes, the anti-CRISPR-sgRNA-containing fluorescence expression cassettes were cloned into the pSUI-SynP-CAPsg or pSUI-SynP-sfGFPsg using Biobrick assembly.

Optical Density and Fluorescence Measurement. For different combinational designs, a 200 μL broth was taken and put into a 96-well plate. The optical density for biomass was measured at the wavelength of 600 nm, and the sfGFP fluorescence was attained by excitation at 480 nm and emission at 510 nm using SpectraMax M2Microplate Readers (Molecular Devices, Sunnyvale, CA).

Data Analysis. The dose−response curve of basic circuits was modeled by Hill's equation as follows.

$$y = y_0 + \frac{ax^b}{c^b + x^b}$$

Here, y denotes the specific fluorescence value corresponding to the concentration of targeted analytes at the level x. y_0 represents the basal or leakage expression of the inducible promoter using the same unit as y. a is the dynamic range and indicates the strength of the inducible promoter. c represents the concentration resulting in half-maximal induction, and b is the Hill coefficient.[11] All parameters (*i.e.*, a, b, c, and y_0) can be estimated by fitting the experimental data *via* SigmaPlot 12.1 software (Systat Software, San Jose, CA) according to the manufacturer's instructions. Nonlinear or linear least-squares regression was used to minimize error between the fitted and experimental data.

Real-Time Detection in Microsystem. Bacteria were precultured in 3 mL LB medium for 12 h. A 180 μL MM9 medium with different concentrations of glucose was first put into a 96-well plate. Afterward, a 20 μL broth was inoculated into each well. The culture was performed in the 37 °C incubator and shaken at 200 rpm. The biomass and fluorescence intensity were measured once an hour until 12 h.

Sensing Urine Glucose in the Microdevice. For the microdevice examination, the cell was first cultivated and then concentrated to an OD_{600} of 20. A 20 μL concentrated cell was inoculated into the microdevice which contained the 180 μL artificial urine solution (0.4 g/L $CaCl_2$, 0.29 g/L $MgCl_2$, 4.22 g/L NaCl, 2.06 g/L Na_2SO_4, 0.57 g/L $Na_2C_6H_5O_7$, 0.02 g/L $Na_2C_2O_4$, 2.54 g/L KH_2PO_4, 1.44 g/L KCl, 0.92 g/L NH_4Cl, 0.25 g/L urea, 1.22 g/L creatine) with different glucose concentrations.[40] After culturing for 12 h, the microdevice was slightly centrifuged to collect the cell onto the membrane and the artificial urine solution was filtered into the lower section of the microdevice. The cell was illuminated by the blue LED flashlight to observe the fluorescence.

■ ASSOCIATED CONTENT

Supporting Information

The Supporting Information is available free of charge at https://pubs.acs.org/doi/10.1021/acssynbio.1c00014.

Supplementary figure (S1) illustrated the NIMPLY logic gate; Supplementary tables detailing of oligonucleotides

https://dx.doi.org/10.1021/acssynbio.1c00014
ACS Synth. Biol. 2021, 10, 412−421

(S1) primers, and (S2) genetic element used in this work (PDF)

AUTHOR INFORMATION

Corresponding Author

I-Son Ng − *Department of Chemical Engineering, National Cheng Kung University, Tainan 701, Taiwan;* orcid.org/0000-0003-1659-5814; Phone: +866-62757575; Email: yswu@mail.ncku.edu.tw; Fax: +86-62344496

Author

Shih-I Tan − *Department of Chemical Engineering, National Cheng Kung University, Tainan 701, Taiwan;* orcid.org/0000-0002-7632-9991

Complete contact information is available at: https://pubs.acs.org/10.1021/acssynbio.1c00014

Author Contributions

SIT and ISN conceived the study. SIT performed all the experiments and original draft investigation. ISN did methodology validation, supervised the experiments, prepared, reviewed, and edited the manuscript.

Notes

The authors declare no competing financial interest.

ACKNOWLEDGMENTS

The authors are grateful to the financial support for this study provided by the Ministry of Science and Technology (MOST 108-2221-E-006-004-MY3 and MOST 108-2218-E-006-006) in Taiwan. The authors also appreciated Ruei-En Hu, Jie-Yao Yu, and Yi-Jun Lan to support the experiments.

REFERENCES

(1) Wan, X., Volpetti, F., Petrova, E., French, C., Maerkl, S. J., and Wang, B. (2019) Cascaded amplifying circuits enable ultrasensitive cellular sensors for toxic metals. *Nat. Chem. Biol. 15* (5), 540−548.

(2) Wang, B., Barahona, M., and Buck, M. (2013) A modular cell-based biosensor using engineered genetic logic circuits to detect and integrate multiple environmental signals. *Biosens. Bioelectron. 40* (1), 368−376.

(3) Kim, H. J., Lim, J. W., Jeong, H., Lee, S. J., Lee, D. W., Kim, T., and Lee, S. J. (2016) Development of a highly specific and sensitive cadmium and lead microbial biosensor using synthetic CadC-T7 genetic circuit. *Biosens. Bioelectron. 79*, 701−708.

(4) Woo, S. G., Moon, S. J., Kim, S. K., Kim, T. H., Lim, H. S., Yeon, G. H., Sung, B. H., Lee, C. H., Lee, S. G., Hwang, J. H., and Lee, D. H. (2020) A designed whole-cell biosensor for live diagnosis of gut inflammation through nitrate sensing. *Biosens. Bioelectron. 168*, 112523.

(5) Gurbatri, C. R., Lia, I., Vincent, R., Coker, C., Castro, S., Treuting, P. M., Hinchliffe, T. E., Arpaia, N., and Danino, T. (2020) Engineered probiotics for local tumor delivery of checkpoint blockade nanobodies. *Sci. Transl. Med. 12* (530), eaax0876.

(6) Lalwani, M. A., Ip, S. S., Carrasco-López, C., Day, C., Zhao, E. M., Kawabe, H., and Avalos, J. L. (2021) Optogenetic control of the lac operon for bacterial chemical and protein production. *Nat. Chem. Biol. 17*, 71−79.

(7) Xu, X., Li, X., Liu, Y., Zhu, Y., Li, J., Du, G., Chen, J., Ledesma-Amaro, R., and Liu, L. (2020) Pyruvate-responsive genetic circuits for dynamic control of central metabolism. *Nat. Chem. Biol. 16*, 1261−1268.

(8) Saltepe, B., Kehribar, E. S., Su Yirmibeşoğlu, S. S., and Şafak Şeker, U. O. (2018) Cellular biosensors with engineered genetic circuits. *ACS Sens. 3* (1), 13−26.

(9) Lim, H. G., Jang, S., Jang, S., Seo, S. W., and Jung, G. Y. (2018) Design and optimization of genetically encoded biosensors for high-throughput screening of chemicals. *Curr. Opin. Biotechnol. 54*, 18−25.

(10) Lopreside, A., Wan, X., Michelini, E., Roda, A., and Wang, B. (2019) Comprehensive profiling of diverse genetic reporters with application to whole-cell and cell-free biosensors. *Anal. Chem. 91* (23), 15284−15292.

(11) Tan, S. I., and Ng, I. S. (2020) New insight into plasmid-driven T7 RNA polymerase in *Escherichia coli* and use as a genetic amplifier for a biosensor. *ACS Synth. Biol. 9* (3), 613−622.

(12) Meyer, A. J., Segall-Shapiro, T. H., Glassey, E., Zhang, J., and Voigt, C. A. (2019) *Escherichia coli* "Marionette" strains with 12 highly optimized small-molecule sensors. *Nat. Chem. Biol. 15* (2), 196−204.

(13) Shin, J., Zhang, S., Der, B. S., Nielsen, A. A., and Voigt, C. A. (2020) Programming *Escherichia coli* to function as a digital display. *Mol. Syst. Biol. 16* (3), e9401.

(14) Wu, P., Chen, Y., Liu, M., Xiao, G., and Yuan, J. (2021) Engineering an optogenetic CRISPRi platform for improved chemical production. *ACS Synth. Biol. 10*, 125.

(15) Whiting, D. R., Guariguata, L., Weil, C., and Shaw, J. (2011) IDF diabetes atlas: global estimates of the prevalence of diabetes for 2011 and 2030. *Diabetes Res. Clin. Pract. 94* (3), 311−321.

(16) Wang, H. C., and Lee, A. R. (2015) Recent developments in blood glucose sensors. *J. Food Drug Anal 23* (2), 191−200.

(17) Miyashita, M., Ito, N., Ikeda, S., Murayama, T., Oguma, K., and Kimura, J. (2009) Development of urine glucose meter based on micro-planer amperometric biosensor and its clinical application for self-monitoring of urine glucose. *Biosens. Bioelectron. 24* (5), 1336−1340.

(18) Kim, J., Campbell, A. S., and Wang, J. (2018) Wearable non-invasive epidermal glucose sensors: A review. *Talanta 177*, 163−170.

(19) Rogers, J. K., Guzman, C. D., Taylor, N. D., Raman, S., Anderson, K., and Church, G. M. (2015) Synthetic biosensors for precise gene control and real-time monitoring of metabolites. *Nucleic Acids Res. 43* (15), 7648−7660.

(20) Dumay, V., Danchin, A., and Crasnier, M. (1996) Regulation of *Escherichia coli* adenylate cyclase activity during hexose phosphate transport. *Microbiology 142* (3), 575−583.

(21) Tsai, M. J., Wang, J. R., Yang, C. D., Kao, K. C., Huang, W. L., Huang, H. Y., Tseng, C. P., Huang, H. D., and Ho, S. Y. (2018) PredCRP: predicting and analysing the regulatory roles of CRP from its binding sites in *Escherichia coli*. *Sci. Rep. 8*, 951.

(22) Ito, N., Miyashita, M., and Ikeda, S. (2019) Portable urine glucose sensor. In *Chemical, Gas, and Biosensors for Internet of Things and Related Applications* (Mitsubayashi, K., Niwa, O., and Ueno, Y., Eds.) pp 3−12, Elsevier.

(23) Chen, X. F., Xia, X. X., Lee, S. Y., and Qian, Z. G. (2018) Engineering tunable biosensors for monitoring putrescine in *Escherichia coli*. *Biotechnol. Bioeng. 115* (4), 1014−1027.

(24) Clifton, K. P., Jones, E. M., Paudel, S., Marken, J. P., Monette, C. E., Halleran, A. D., Epp, L., and Saha, M. S. (2018) The genetic insulator RiboJ increases expression of insulated genes. *J. Biol. Eng. 12* (1), 1−6.

(25) Lou, C., Stanton, B., Chen, Y. J., Munsky, B., and Voigt, C. A. (2012) Ribozyme-based insulator parts buffer synthetic circuits from genetic context. *Nat. Biotechnol. 30* (11), 1137.

(26) Carrier, T. A., and Keasling, J. D. (1997) Engineering mRNA stability in *E. coli* by the addition of synthetic hairpins using a 5′ cassette system. *Biotechnol. Bioeng. 55* (3), 577−580.

(27) Qi, L. S., Larson, M. H., Gilbert, L. A., Doudna, J. A., Weissman, J. S., Arkin, A. P., and Lim, W. A. (2013) Repurposing CRISPR as an RNA-guided platform for sequence-specific control of gene expression. *Cell 152* (5), 1173−1183.

(28) Wang, T., Guan, C., Guo, J., Liu, B., Wu, Y., Xie, Z., Zhang, C., and Xing, X. H. (2018) Pooled CRISPR interference screening enables genome-scale functional genomics study in bacteria with superior performance. *Nat. Commun.*, DOI: 10.1038/s41467-018-04899-x.

(29) Tan, S. I., Yu, P. J., and Ng, I. S. (2020) CRISPRi-mediated programming essential gene *can* as a Direct Enzymatic Performance Evaluation & Determination (DEPEND) system. *Biotechnol. Bioeng. 117* (9), 2842−2851.
(30) Hawkins, J. S., Wong, S., Peters, J. M., Almeida, R., and Qi, L. S. (2015) Targeted Transcriptional Repression in Bacteria Using CRISPR Interference (CRISPRi). In *CRISPR. Methods in Molecular Biology* (Lundgren, M., Charpentier, E., and Fineran, P., Eds.) Vol. *1311*, pp 349−362, Humana Press, New York, NY.
(31) Kampmann, M. (2018) CRISPRi and CRISPRa screens in mammalian cells for precision biology and medicine. *ACS Chem. Biol. 13* (2), 406−416.
(32) Larson, M. H., Gilbert, L. A., Wang, X., Lim, W. A., Weissman, J. S., and Qi, L. S. (2013) CRISPR interference (CRISPRi) for sequence-specific control of gene expression. *Nat. Protoc. 8* (11), 2180−2196.
(33) Pickar-Oliver, A., and Gersbach, C. A. (2019) The next generation of CRISPR-Cas technologies and applications. *Nat. Rev. Mol. Cell Biol. 20* (8), 490−507.
(34) Sandberg, T. E., Salazar, M. J., Weng, L. L., Palsson, B. O., and Feist, A. M. (2019) The emergence of adaptive laboratory evolution as an efficient tool for biological discovery and industrial biotechnology. *Metab. Eng. 56*, 1−16.
(35) Lee, Y. J., Hoynes-O'Connor, A., Leong, M. C., and Moon, T. S. (2016) Programmable control of bacterial gene expression with the combined CRISPR and antisense RNA system. *Nucleic Acids Res. 44* (5), 2462−2473.
(36) Studier, F. W., and Moffatt, B. A. (1986) Use of bacteriophage T7 RNA polymerase to direct selective high-level expression of cloned genes. *J. Mol. Biol. 189* (1), 113−130.
(37) Wang, W., Li, Y., Wang, Y., Shi, C., Li, C., Li, Q., and Linhardt, R. J. (2018) Bacteriophage T7 transcription system: an enabling tool in synthetic biology. *Biotechnol. Adv. 36* (8), 2129−2137.
(38) Tan, S. I., You, S. C., Shih, I. T., and Ng, I. S. (2020) Quantification, regulation and production of 5-aminolevulinic acid by green fluorescent protein in recombinant *Escherichia coli*. *J. Biosci. Bioeng. 129* (4), 387−394.
(39) Otten, J., Tenhaef, N., Jansen, R. P., Döbber, J., Jungbluth, L., Noack, S., Oldiges, M., Wiechert, F., and Pohl, M. (2019) A FRET-based biosensor for the quantification of glucose in culture supernatants of mL scale microbial cultivations. *Microb. Cell Fact. 18* (1), 1−10.
(40) Griffith, D. P., Musher, D. Á., and Itin, C. (1976) Urease. The primary cause of infection-induced urinary stones. *Invest. Urol. 13* (5), 346−350.

https://dx.doi.org/10.1021/acssynbio.1c00014
ACS Synth. Biol. 2021, 10, 412−421